Path optimization for uniform removal pre-polishing of optical glass with industrial robots

Liangxiao Zhao,[a,b] **Jian Zhang**,[a,c,*] **and Limin Gao**[a]
[a]Xi'an Institute of Optics and Precision Mechanics of CAS, Xi'an, China
[b]University of Chinese Academy of Sciences, Beijing, China
[c]Xidian University, School of Mechano-Electronic Engineering, Xi'an, China

Abstract. In the field of precision optical manufacturing, the manufacturing method using industrial robots as the carrier has highlighted its advantages of being more economical and efficient than existing methods. The application of different end-effectors has expanded the scenarios and processing limits of optical polishing. However, concise and simplified polishing technologies remain challenging. To improve the versatility of industrial robots in different processes and reduce the number of polishing iterations, pre-polishing with uniform removal is introduced and optimized, providing an excellent basic surface for polishing and finishing. Combined with the performance of an industrial robot, we adopt a swing composite path, to which the motion parameters are adjusted and optimized to minimize the fluctuation of the overall overlap rate (within 5%). The optimal path is based on the uniform B-spline curve characterization, which improves the consistency of the dwelling time and reduces the complexity of pre-polishing, laying a theoretical foundation for efficient and high-quality optical manufacturing.
 [DOI: 10.1117/1.OE.61.4.045104]

Keywords: pre-polishing; uniform removal; swing composite path; overlap rate.

Paper 20211548G received Jan. 7, 2022; accepted for publication Apr. 4, 2022; published online Apr. 20, 2022.

1 Introduction

As optical systems continue to prosper in diverse application fields, their increasing complexity poses new challenges to ultra-precision optical elements, specifically medium- and large-sized optical glass. For the manufacturing technology of optical glass, classical processes including milling, grinding, and polishing have been widely used.[1] Among them, polishing accounts for the largest proportion of the total production time, for which tremendous efforts have been made in terms of innovative technologies and methodologies. Throughout the manufacturing process of optical glass, the machining accuracy, surface quality of glass, and processing efficiency have been jointly optimized through various technology renewal, iteration, and improvement processes. These efforts involve computer-controlled optical surfacing (CCOS) technology,[2] magnetorheological finishing (MRF),[3] ion beam figuring,[4] and jet polishing.[5] In reality, overall production efficiency not only depends on a certain single production link but requires more reasonable and scrupulous coordination among all manufacturing procedures. Particularly during mass production, the performance limitations of diverse production equipment may hinder the implementation of state-of-the-art research. To achieve the expected accuracy, an emerging research trend that simplifies the manufacturing method by further subdividing the process flow has attracted much attention.

The introduction of pre-polishing is one of the important ideas for which the earliest description can be traced back to the study by Dumas et al.[6] in 2007. They adopted mechanical polishing as a reference to create an optical pre-polishing link according to the characteristics of different manufacturing methods and conditions, which reduced the potential surface damage generated during milling. By combining MRF and small-tool polishing, Dumas et al. succeeded in manufacturing a special-shaped mirror. Kiontke and Steinkopf[7] summarized the related issues of

*Address all correspondence to Jian Zhang, zj@opt.ac.cn

aspherical manufacturing based on practical experiences and emphasized the importance and goals of pre-polishing, which can be outlined as reducing roughness and retaining surface accuracy.

Despite these studies, few researches have focused on pre-polishing. Zhong et al.[8] studied the effect of adding a pre-polishing procedure on wafer manufacturing, particularly on the flatness of the wafer. In 2015 and 2016, Chaves-Jacob et al.[9] studied the pre-polishing of mechanical parts based on a five-axis computerized numerical control (CNC) machine, which had critical reference to optical polishing. Recently, Wang et al.[10] and Ke et al.[11] proposed a pre-polishing method that used a semi-rigid bonnet and reduced the edge effect, providing a new perspective for optical pre-polishing. Furthermore, Zhong et al.[12] introduced the evaluation and compensation of kinematic error in robot-based bonnet polishing during pre-polishing, which corrected the kinematic error of the robot while improving the pre-polishing accuracy. Zeeko conducted extensive research on optical polishing equipment, its specialist Prochaska[13] reported the excellent performance of pre-polishing in removing sub-surface damage.

In addition to the aforementioned studies, Liu et al.[14] conducted a study on the spiral path and Feng et al.[15] conducted a study on the distortion of line spacing of an aspheric spiral path, which simplified the implementation of optical polishing. Unfortunately, these studies depended heavily on CNC machines and focused primarily on the impact of pre-polishing on the entire process and on the polishing procedure, which may pose a potential hindrance to the mass manufacturing of optical glass. After clarifying the positive effects of pre-polishing, a unified evaluation criterion is required to simplify and optimize the path during pre-polishing.

Combining the path optimization of optical polishing in CCOS and the outstanding characteristics of industrial robots as actuators, we use a uniform pre-polishing path with a uniform B-spline curve as the speed variation characteristic before polishing and finishing. Specifically, a polishing end-effector designed by us is installed on an industrial robot, to which a simple but efficient path is adopted. Moreover, we introduce an ideal surface foundation for polishing to further minimize the number of iterations, improving the manufacturing efficiency of the optical glass. The proposed method can greatly reduce path points, exhibiting excellent operability in practical applications.

The remainder of this paper is organized as follows. Section 2 formulates the rationale for the uniform removal and the fundamental of path planning. Section 3 presents the optimization method and simulation machining. Section 4 outlines the structure and components of the optical polishing system of an industrial robot and presents the experimental results and analysis. Finally, Sec. 5 summarizes the conclusions of the study.

2 Fundamental of Uniform Pre-Polishing

2.1 *Basis of Composite Polishing*

The initial surface to be polished directly affects the frequency and extent of the mid- and high-frequency errors. The base surface directly determines the location of the processing wall. The processing wall can be defined as the best surface accuracy that can be realized using existing polishing technologies in an economical manner. Therefore, streamlined and reasonable pre-polishing not only improves the basic surface shape after grinding but also increases the efficiency of the entire process.

Figure 1 shows a schematic of the pre-polishing system used in this study, where the workpiece is fixed on the turntable by negative pressure and is positioned coaxially with the turntable. The workpiece rotates with the turntable. The polishing head moves along the generatrix of the workpiece. The composite path covers the entire surface of the workpiece. Compared with paths such as grating and pseudorandom, this path simplifies the motion complexity of the actuator to the greatest extent, through which the stability of the path is improved. This pre-polishing path is also equivalent to a spiral path.

Although introducing optical manufacturing into the application of industrial robots can significantly reduce costs, the fundamental performance of industrial robots as carriers must be considered. In this study, the proposed simplified composite motion facilitates more accessible

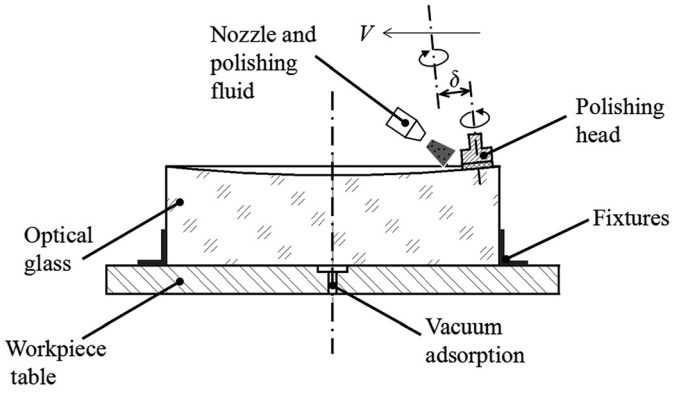

Fig. 1 Schematic of the pre-polishing system.

deploying and implementation of industrial robots. Compared with the numerical control codes of multi-axis machine tools, the post-code of industrial robots has a significantly lower load capacity.[16] Most industrial robot control systems exhibit inadequate stability when running tens of thousands of lines of code; under these circumstances, the teaching pendant system may even report errors, and it cannot be executed. The conventional path of large-aperture optical elements contains tens of thousands of lines, specifically for high-order aspheric surfaces or free-form surfaces, which necessitates the aforementioned research on the simplified composite path. When manufacturing rotationally symmetric optical glass or certain irregular-shaped or off-axis optical glass, a parent mirror based on rotational symmetry is used. When polishing is finished or the surface shape of the mirror is close to the target, the workpiece is processed into the expected shape. Therefore, the majority of machining goals can be achieved using rotation symmetric machining methods before conducting the polishing process, which further enables the feasibility of the proposed pre-polishing method.

Specifically, we adopt a method in which an industrial robot drives the end-effector to swing the generatrix with the rotating workpiece to complete the pre-polishing path composite. The machining center of the end-effector is called the tool center point (TCP).[17] To identify the continuity of motion, the TCP moves inward from the outside of the workpiece to the center along the generatrix, in which a single swing motion is defined as one pre-polishing motion unit. The TCP moves according to the equation, which is given by

$$r = R_{\text{glass}} - f(t) \quad \begin{cases} x = r\cos\omega t \\ y = r\sin\omega t \\ z = \dfrac{cr^2}{1+\sqrt{1-(1+k)c^2r^2}} \end{cases}, \tag{1}$$

where r is the radial position, R_{glass} is the radius of the outer circumference of the workpiece, $f(t)$ is the distance function of the swing motion, t is the time of the motion unit, x, y, and z are the space coordinates of the TCP, ω is the angular velocity of the workpiece rotating with the turntable, k is the function of the eccentricity of the quadratic surface, and c is the paraxial curvature of the vertex. Figure 2 shows the composite path covering the mirror surface, where the red and dotted black lines represent the composite path and swing path, respectively. To obtain a continuous Gaussian-shaped removal function in motion, the revolution speed within step time T should be greater than $60/T$.

2.2 *Evaluation Indicator of the Path*

When the classical Archimedes path is used for full-caliber polishing, the phenomenon of center overcutting occurs. Thus, the mirror surface becomes funnel-shaped, which destroys the basic surface. When the turntable and swing move at a constant speed, the composite path forms an Archimedes spiral, which must be avoided. Therefore, variable-speed rotation and swing are required. Unfortunately, in practical production, an inadequate speed-varying capacity of the

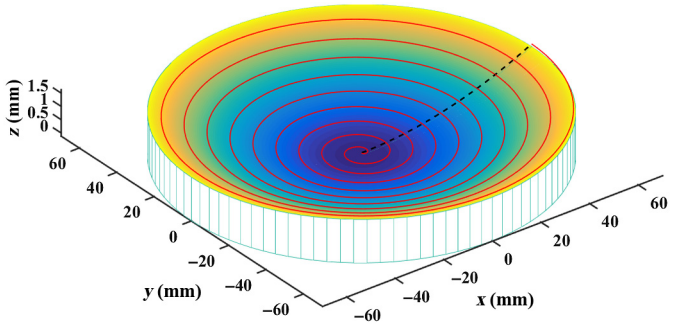

Fig. 2 Composite path.

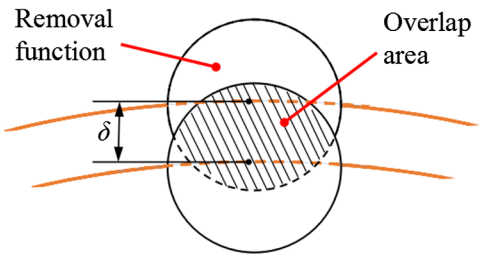

Fig. 3 Overlap area along the radial direction.

turntable can cause the speed truncation phenomenon. Given the above situation, the speed variation of the swing must be evaluated from a macro perspective in terms of certain specific and unified indices. The nature of the surface error caused by overcutting and missed cutting is the difference in the amount of tool removal. In deterministic polishing, the removal amount is usually expressed by the dwelling time of the tool staying on the workpiece. In this study, we use the coverage rate instead of the dwelling time to express the removal amount. The overlap area along the radial direction is shown in Fig. 3.

By changing the two variables according to the following equation, the composite path can be simulated as a spiral with a different pitch. The pitch δ of the composite path can be calculated by the substitution operation of Eq. (1), which is given as

$$\delta = \frac{2\pi V}{\omega}. \tag{2}$$

In Eq. (2) and the simulation, the pitch of the spiral is positively correlated with the swing speed V of the generatrix, and it is negatively correlated with the rotation speed of the workpiece ω. The pitch of a spiral directly affects the coverage difference of the removal function between steps.

To describe the effect of spiral pitch on material removal, the overlap rate of the polishing area (radial overlap rate) of two adjacent rows of polishing tools can be calculated according to the ratio of the overlap area to the effective removal area of polishing tools. The overlap rate is constant on a two-dimensional projection with a fixed spiral pitch. The calculation result is represented by α, which can be expressed as

$$\alpha = \frac{2\left(\pi R_{\text{removal}}^2 \frac{\arccos \frac{\delta}{2R_{\text{removal}}}}{180\ \text{deg}} - \sqrt{R_{\text{removal}}^2 - \frac{\delta^2}{4}}\frac{\delta}{2}\right)}{\pi R_{\text{removal}}^2}, \tag{3}$$

where R_{removal} is the radius of the removal function. Subsequently, by substituting Eq. (2) into Eq. (3), we obtain

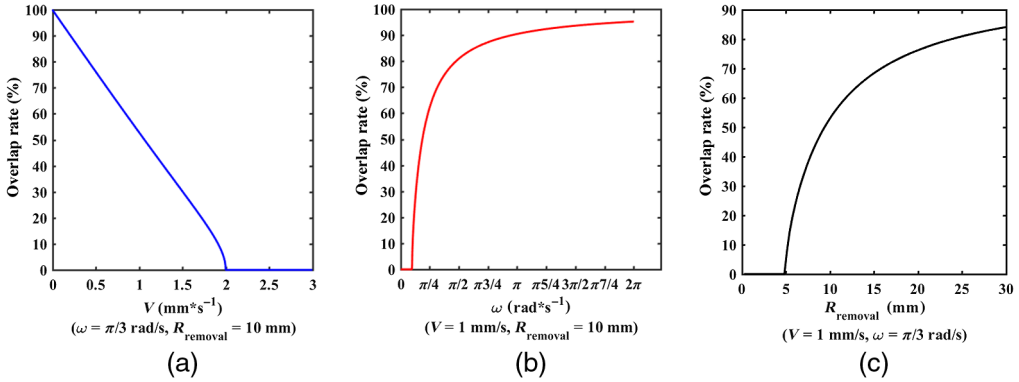

Fig. 4 Univariate variation trend of radial overlap rate: (a) swing speed, (b) rotation speed, and (c) radius of the removal function.

$$\alpha = \frac{\arccos \frac{\pi V}{\omega R_{\text{removal}}}}{90 \text{ deg}} - \sqrt{R_{\text{removal}}^2 - \frac{\pi^2 V^2}{\omega^2}} \frac{\pi V}{\omega \pi R_{\text{removal}}^2}. \tag{4}$$

There are three main factors affecting the radial overlap rate α: V, ω, and R_{removal}. The variation trend of the overlap rate α affected by different parameters is shown in Fig. 4.

The three factors impose different effects on the overlap rate. In addition to the negative correlation of the swing velocity, the positive influence of rotation speed and radius of the removal function on the overlap rate have a relatively smooth range, based on the first evaluation indicator obtained. However, regardless of any parameters selected for pre-polishing based on analysis and equipment conditions, the center area of the mirror is lower than the outer area, and more material is removed in the central area. This finding also originates from the manufacturing experience. Apart from the aforementioned radial overlap rate, the overlap rate along the path direction should be considered.

Thereafter, we define s as the length of the path drawn by the center of the removal function in the step time, as shown in Fig. 5.

By calculating the curve integral of the arc length, the value is expressed as

$$\int_L f(x,y,z)\mathrm{d}s = \int_a^b f[\varphi(t),\phi(t),\Omega(t)]\sqrt{\varphi'^2(t)+\phi'^2(t)+\Omega'^2(t)}\mathrm{d}t \ (a<t<b), \tag{5}$$

where φ, ϕ, and Ω denote the parametric equations of variables x, y, and z of the space curve, respectively, and the parametric equation of the composite path can be obtained according to Eq. (1), a and b are the upper and lower bounds of parametric variable t, respectively. When $f(x,y,z) = 1$, the calculation result is the length of the space curve, which is expressed as

$$s = \int_a^b \sqrt{x'^2(t)+y'^2(t)+z'^2(t)}\mathrm{d}t \ (a<t<b). \tag{6}$$

The step time is the time the polishing tool takes to move 1 mm, and the path length s in step time is equivalent to the central connection line of the polishing area along the path direction, i.e.,

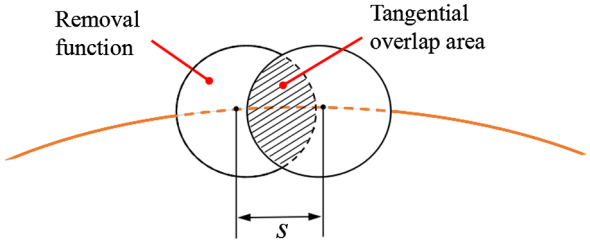

Fig. 5 Overlap area along the tangent direction.

the distance δ. The tangential overlap rate β can be obtained by substituting it into Eq. (3). Combining the two effects imposed on different surface types, we obtain a comprehensive overlap rate, which is given by

$$\xi = \kappa_1 \alpha + \kappa_2 \beta, \quad \kappa_1, \kappa_2 \in (0,1), \tag{7}$$

where κ_1 and κ_2 are the coefficients of a and β, respectively, i.e., the contribution rate to ξ.

The rationality of the composite path of pre-polishing and its motion can be analyzed and optimized to improve coverage consistency, thereby realizing uniform material removal.

3 Path Optimization and Machining Simulation

The above analysis and problems in actual production suggest that inconsistent material removal occurs in the uniform Archimedes spiral path. To solve this problem, we set the initial velocity of uniform acceleration and the final velocity of uniform deceleration to 0 and substitute the final velocity of uniform acceleration and initial velocity of uniform deceleration V_f and total duration of the motion unit t_{all} into the basic kinematics formula ($S_t = v_0 t + \frac{1}{2} a t^2$ and $v = v_0 + at$, where S_t is the distance, v_0 is the initial velocity, a is the acceleration, t is the time, and v is the velocity at t). Then, let $f(t) = S_t$, we substitute S_t into Eq. (1) to obtain the uniform acceleration and deceleration motion laws of the position–time, which are given by

$$\begin{cases} r = R_{\text{glass}} - \frac{V_f}{2t_{\text{all}}} t^2 \\ r = R_{\text{glass}} - V_f t + \frac{V_f}{2t_{\text{all}}} t^2 \end{cases}. \tag{8}$$

We set the swing motion as a variable-speed motion with constant acceleration, by which the speed variation obeys the aforementioned two rules.

MATLAB software is used to generate the composite path of the mirror, as shown in Fig. 6. It is observed from Fig. 6(b) that the outer pitch is larger than the size of the removal function, which may result in missed cutting. The reduction in pitch during deceleration causes inconsistencies in the overlap rate. By contrast, the acceleration situation shown in Fig. 6(a) is more in line with the goals and requirements of uniform removal. Concurrently, the comprehensive overlap rate as an evaluation index should be optimized, upon which machining simulation should also be implemented to verify the rationality of the optimization further intuitively.

Therefore, the variable-speed method of a swing directly affects the consistency of the composite path and material removal. By substituting the variable-speed equation of the uniformly accelerated swing into the composite path equation, the pitch can be obtained as

$$\delta = \frac{2R_{\text{glass}}}{t_{\text{all}}^2}. \tag{9}$$

Substituting Eq. (9) into Eq. (3), we obtain

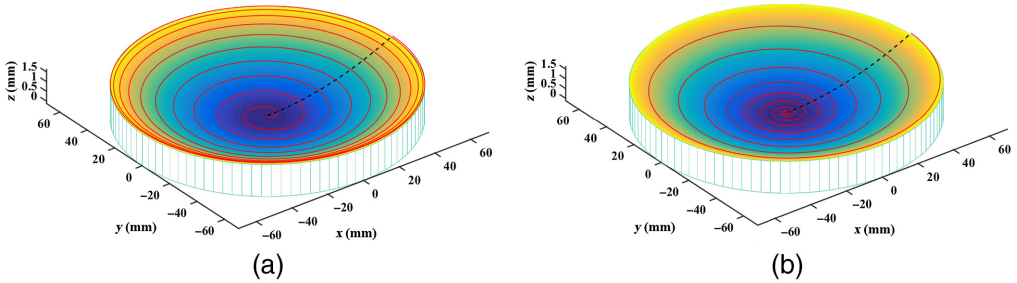

Fig. 6 Variable-speed composite path: (a) accelerated composite path and (b) decelerated composite path.

$$\alpha = \frac{2\left(\pi R_{\text{removal}}^2 \frac{\arccos \frac{R_{\text{glass}}}{t_{\text{all}}^2 R_{\text{removal}}}}{180\ \text{deg}} - \sqrt{R_{\text{removal}}^2 - \frac{R_{\text{glass}}^2}{t_{\text{all}}^4}} \frac{R_{\text{glass}}}{t_{\text{all}}^2}\right)}{\pi R_{\text{removal}}^2}. \tag{10}$$

The tangent length s is

$$s = \int_a^b \sqrt{\frac{\omega^2 R_{\text{glass}}^2}{t_{\text{all}}^4}(t^4 - 2t_{\text{all}}^2 t^2) + \frac{4R_{\text{glass}}^2}{t_{\text{all}}^4} + \omega^2 R_{\text{glass}}^2}\,\mathrm{d}t. \tag{11}$$

Subsequently, we substitute s into Eq. (3) and calculate the best t_{all} according to the comprehensive overlap rate equation. The variation in the radial overlap rate, tangential overlap rate, and comprehensive overlap rate with time t was calculated using MATLAB software, and the optimal variation trend of the overlap rate was obtained through optimization calculations, as shown in Fig. 7. The theoretical comprehensive overlap rate of the entire process of a single swing motion fluctuates within a range of 5% to 10% after optimization.

Notably, during the actual manufacturing, the amount of material removed for grinding and rough polishing is quite large[18]; thus, the surface shape error increases as the manufacturing number increases. This problem has also been reported in many other studies on variable-speed polishing. After conducting simulation machining for 10 motion units, the peak-to-valley value exceeded $20\,\lambda$ ($\lambda = 632.8$ nm). The interferometer cannot obtain images owing to the severe center overcutting.

To adjust the rationality of the variable-speed motion, further fine-tuning is required based on the problems caused by uniform acceleration. Therefore, a uniform B-spline is introduced to optimize the characteristic curve of the uniform acceleration in sections. The B-spline curve equation can be written as

$$p(u) = \sum_{i=0}^{n} d_i N_{i,k}(u) \quad (i = 0,1,2,\ldots,n), \tag{12}$$

where d_i is the control point (coordinates) and $N_{i,k}(u)$ is the i'th k-degree B-spline basis function.

Through continuous connections, the B-spline replaces high-order polynomials with piecewise low-order ones, wherein the curve change rate of its line segments can be controlled by control points.[19–21]

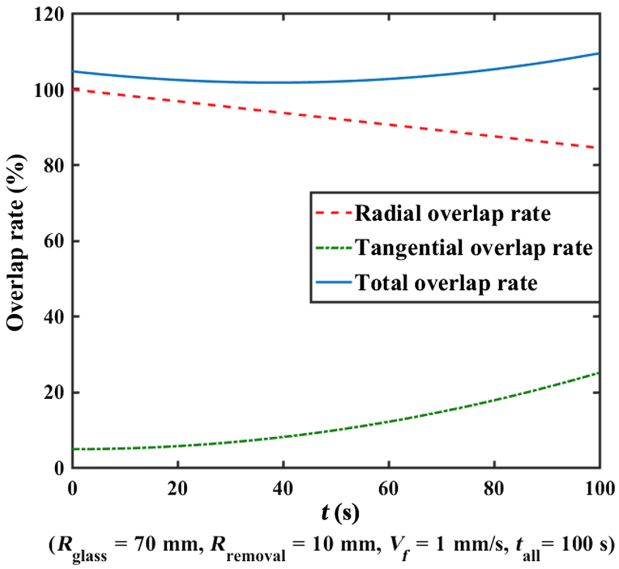

Fig. 7 Variation trend of the overlap rate under variable speed conditions.

First, the intersection of the position–time curve and coordinate axis can be determined according to the R_{glass} of the starting point of the swing motion and the duration of a single motion.

Second, we set five knots to divide the curve into four different segments according to the variation trends of the uniform acceleration motion. For the lower area of the glass, we increase the polishing swing speed by adjusting the slope of the curve, which can reduce the dwelling time and material removal. Conversely, for high regions, the slope of the curve should be decreased to increase the material removal.

Third, we adopt the overlap rate as the evaluation indicator, upon which the control points are set, and segments are optimized. The number and distribution of control points are directly correlated with knots or the characteristics of the glass surface, that is, the distribution of the lower and higher areas and the radius corresponding to the low and high belts. The number of control points should exceed the number of knots. Taking a parabola that represents the curve of optimal uniform acceleration of swing motion as an example, we set four intermediate control points because of the five relatively independent characteristics of the glass surface, which also match the setting of knots. However, note that knots are not control points, and the control points drive segments between knots. The radii corresponding to these four control points are 90% R_{glass}, 75% R_{glass}, 50% R_{glass}, and 15% R_{glass}. Moreover, two outer control points are set with radius values of 110% R_{glass} and −15% R_{glass}. Different speed characteristic curves are obtained by changing the time of the motion to these points, and the proposed overlap rate is used as the evaluation indicator.

Finally, the optimal characteristic curve of the glass is obtained. It can be observed from Fig. 8 that the optimal characteristic curve is located between the uniform speed and uniform acceleration curves, realizing a trade-off between these two curves while achieving comparatively uniform rough polishing.

Because the optimal characteristic curve expresses the relationship between position r and time t, the velocity–time curve can be obtained via derivation. We assign it to an industrial robot that can start pre-polishing after matching the path and velocity–time information in the offline programming software.

The simulation of the pre-polishing verified the excellent performance of the proposed path. Figure 9 shows the simulation results of the uniform velocity, optimal uniform acceleration, and uniform B-spline, during which the tool size, rotating speed, pressure, and polishing environment remain the same. These results are consistent with the analysis of the path overlap rate. Although the central areas of the three simulation results exhibit different degrees of concavity, the optimized pre-polishing proposal achieves a good trade-off between efficiency and quality.

In addition to the above efforts, we analyzed the number of path points. The comparison result of the grating and spiral path suggests that the number of path points introduced in this

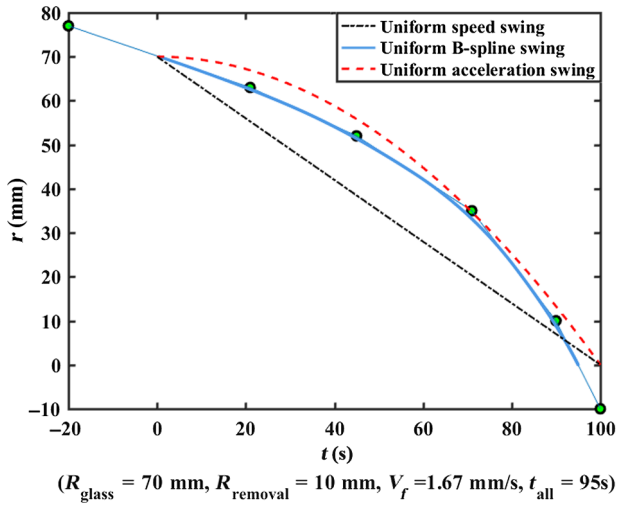

Fig. 8 Three types of velocity characteristic curves.

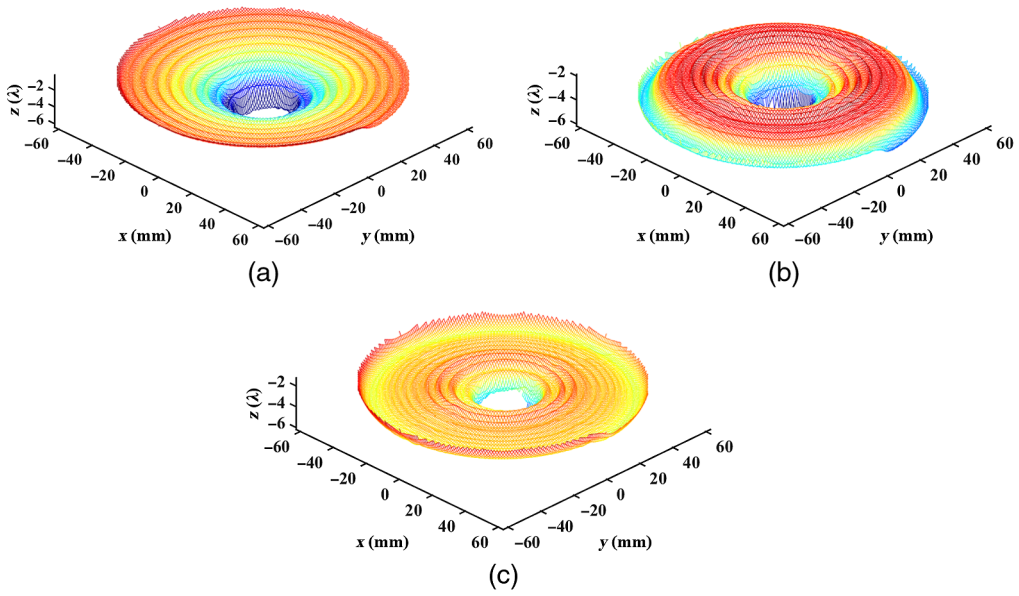

Fig. 9 Simulation polishing in three cases: (a) uniform velocity, (b) optimal uniform acceleration, and (c) uniform B-spline.

study is significantly less than that of the others when the line spacing/spiral pitch and step length are the same. For instance, when we polish a Φ140 mm flat mirror with a line spacing/spiral pitch of 1 mm step length, the path points of a single polishing of the grating path are 15,730, and those of the spiral path is 5760. In contrast, the number of path points of our proposal is 71. When the robot performs an offline program that contains more than 10,000 points, the absolute/relative positioning error of the robot is aggravated. Furthermore, the above program also induces operation errors in the control cabinet, degrading the stability of manufacturing. Therefore, our proposed method outperforms the conventional methods in terms of stability and feasibility.

4 Experiments and Results

To verify the excellent performance of the optimized pre-polishing, we used equipment that is consistent with the actual production. The equipment of industrial robots characterized by the goal of high-efficiency optical manufacturing is required to satisfy multiple-stage demands and thus achieve the goals of pre-polishing and polishing.

4.1 *Experimental Setting*

The experimental equipment we adopted is based on KUKA robot (Model KR210 R2700), which can be equipped with different end-effectors[22] to adapt to different manufacturing stages. Details of the equipment are presented in Fig. 10.

Specifically, an active planetary end-effector was used for pre-polishing in this study. A constant-force cylinder provides the target force and a conductive slip ring and sliding table are used to recognize planetary rotation. The overall structure of the robot is compact and reliable, providing a stable removal function. For the robot, the required pressure, eccentricity, polishing head size, and motor speed are adjustable for different manufacturing scenarios and requirements. The parameters are listed in Table 1.

To demonstrate the uniform removal performance of our proposed pre-polishing method and the basic surface shape prepared for the formal polishing stage, we used a concave spherical K9 mirror with a diameter of 200 mm and a curvature radius of 647 mm. The profile tolerance of surface of the frosted glass is approximately 5 μm. The path longer than that of generatrix of the workpiece is to minimize the edge effect. However, the positive pressure increases when the contact area decreases, and then the removal amount of the removal function increases, resulting

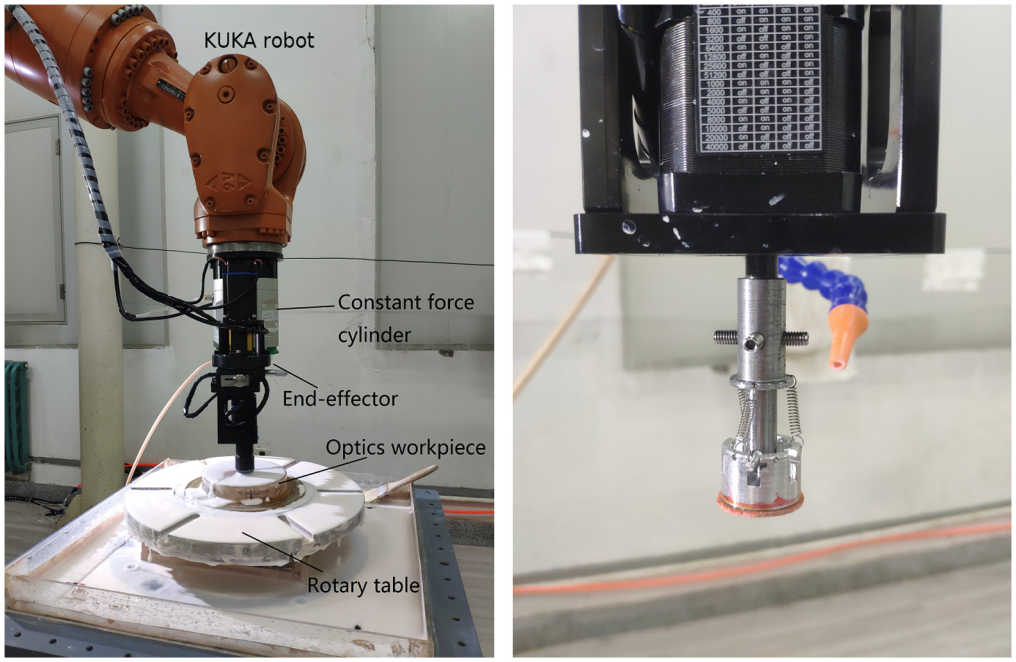

Fig. 10 Equipment of optical polishing robot: (a) polishing robot and (b) floating small tool.

Table 1 Parameters of the polishing robot.

Industrial robot	Model	KUKA KR210 R2700
	Repetitive positioning error	0.02 to 0.2 mm
	Max load	210 kg
End-effector	Velocity range of spin motion	0 to 500 rpm
	Axial stroke	0 to 20 mm
	Force	0 to 100 N
	Optional diameters of the polishing pad	10, 15, and 25 mm

in excessive removal of edge material, which can be referred to as the "edge collapse effect,"[23] thus, the extra part did not exceed half of the range of the removal function.

Specifically, we tested the pre-polishing effect of the mirror surface with the swing motion of uniform speed to demonstrate the accuracy and necessity of the optimized parameters, and we conducted the pre-polishing of the variable-speed swing motion. According to the defined optimization parameters, the necessity for pre-polishing and the better basic surface shape available were determined through the variable-speed path obtained in Sec. 3. Finally, we conducted a comparative experiment to illustrate the effect of pre-polishing on efficiency. The corresponding process parameters are listed in Table 2.

Simultaneously, the tool head of the end-effector must be optimized for the surface curvature of the workpiece. Because the polyurethane has high elasticity, the curvature of the polishing head should be slightly smaller than that of the mirror surface to maximize the effective polishing range and performance. Moreover, the global stability of the removal function depends heavily on constant-force control; therefore, we tested the constant-force performance of the end-effector under dynamic conditions, as shown in Fig. 11.

Table 2 Experimental process parameters.

Tool diameter	10 mm
Pad material	LP66 Polyurethane
Revolution speed	90 rpm
Rotation speed	−250 rpm ("−" denotes reverse)
Force	30 N
Eccentricity (Δ)	4 mm
Workpiece size	Φ200 mm R647 mm spherical surface
Workpiece material	K9
Slurry	12% wt. CeO_2 (with a suspending agent)

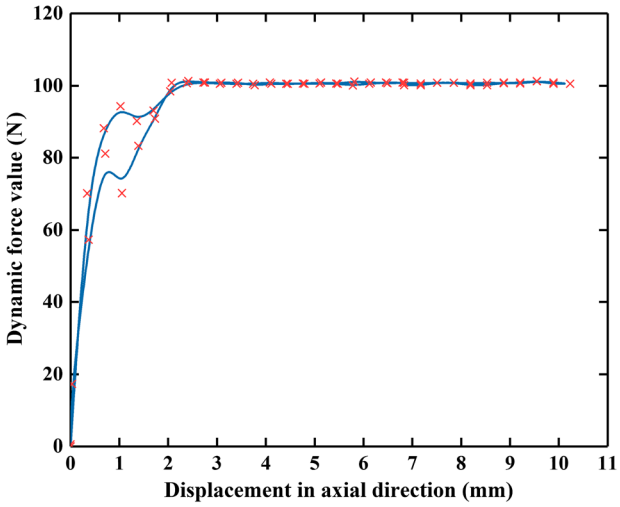

Fig. 11 Constant force of end-effector under dynamic conditions.

4.2 *Experimental Results*

Three experiments were designed to verify the analytical process and results. In the first experiment, multiple uniform motion units were superimposed to illustrate the problem of the removal process, by which the consistency of the simulation machining was verified. The second experiment verified the uniformity of pre-polishing featuring with uniform B-spline speed characteristics. Finally, identical optical glass was polished using the classical method and pre-polishing paths to compare the difference in polishing efficiency.

4.2.1 *Polishing experiment of uniform speed swing*

In this experiment, 10 cycles of pre-polishing were performed (i.e., 10 motion units). The corresponding results are presented in Fig. 12. Using an optical test plate, we discovered that the interference fringes gradually become denser from the outside to the inside. The bending direction of the aperture suggests that the mirror surface has a low spatial-frequency error. The proposed concave trend was consistent with the theoretical analysis, and the curvature of the mirror surface is smaller than the target curvature.

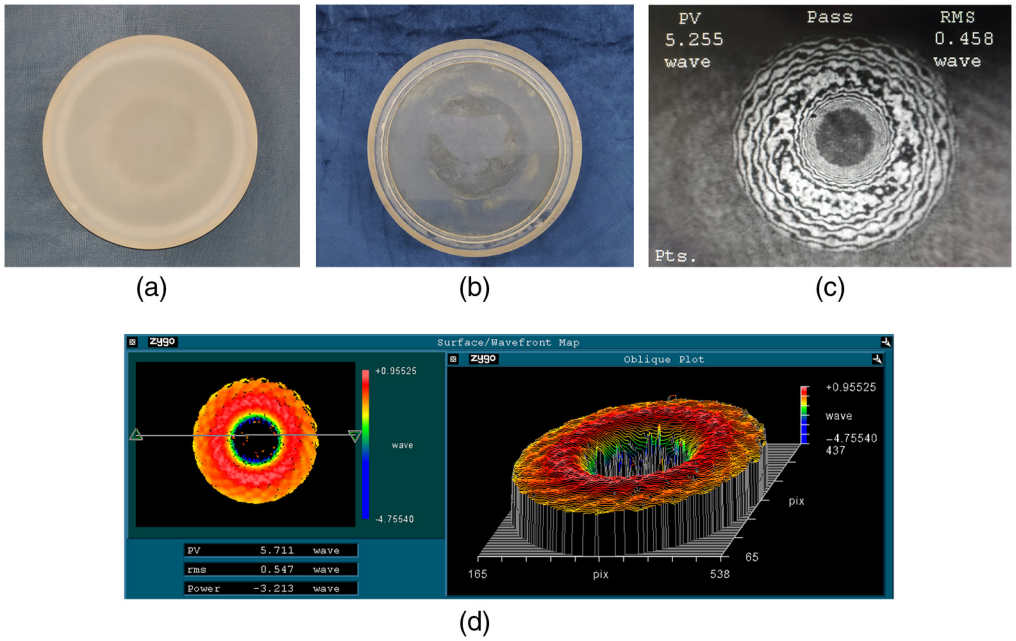

Fig. 12 Experiment results: (a) frosted glass, (b) pre-polished mirror, (c) interference fringes, and (d) surface map.

4.2.2 *Polishing experiment of variable speed swing*

In this experiment, 10 cycles of variable-speed pre-polishing were performed. Considering the actual operating restrictions of the industrial robot, the swing speed was increased from 0 at the edge to 1 mm/s. The imaging area was increased in the interferometer, as shown in Fig. 13, indicating that the problem in the central area was alleviated. The size of the collapse central area accounts for 19% of the entire mirror surface, which is reduced compared to the 35% of the uniform swing pre-polishing shown in Fig. 12(d). In optical design, the center of a mirror is primarily a light hole that must be cut and removed, upon which minimizing the collapsed area, therefore, benefits the optical design. The increase in the power value also suggests that the proposed method will aggravate the convex trend of the surface.

The theoretical analysis suggests that the effective dwelling time of a single polishing of this variable-speed swing is two to three times that of the same uniform-speed swing. Hence, it is necessary to reduce the number of cycles and make the results approximate the processing wall, which can minimize the polishing time and prevent the mid-spatial frequency error from occurring too early. Therefore, we conducted four cycles of pre-polishing experiments with uniform B-spline speed characteristics. The results presented in Fig. 14 indicate that the mid-spatial frequency error was noticeably alleviated, and reducing the number of cycles can further increase

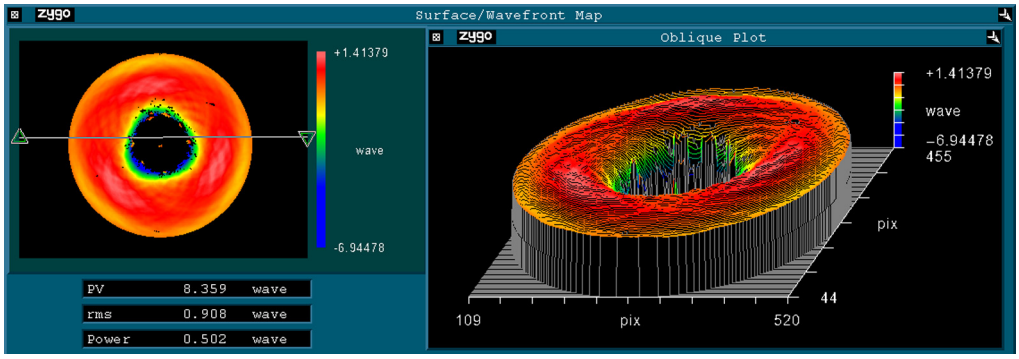

Fig. 13 Result of the uniformly accelerated polishing.

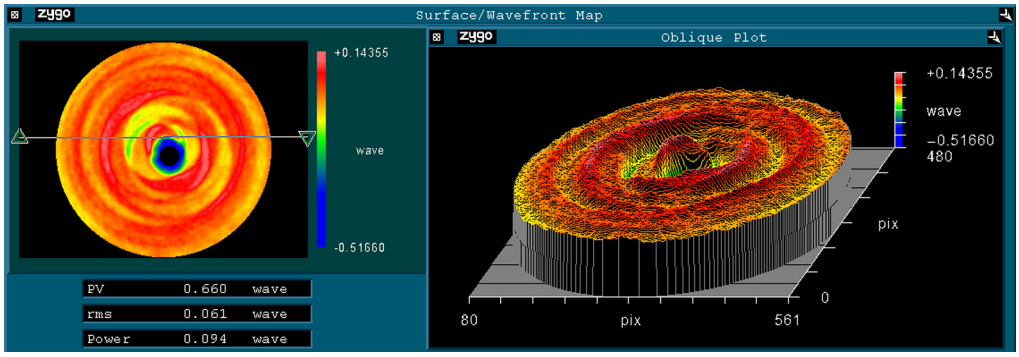

Fig. 14 Result of the uniform B-spline polishing.

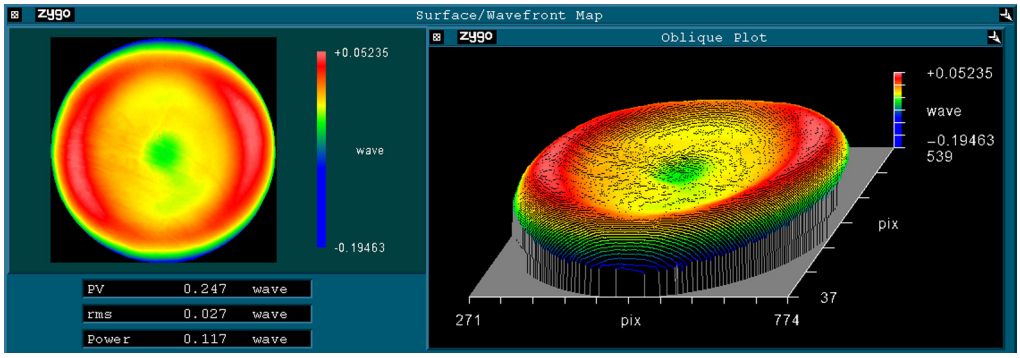

Fig. 15 Final result of the polished mirror.

the process stability. When the root-mean-square (RMS) is approximately 1 λ, the former polishing path induces serious problems in the central area of the mirror, whereas the latter path is much better. Using a uniform B-spline can enable a much lower concave of the mirror within a small area, to which the RMS value is less than $1/15\,\lambda$. Our proposed parameter optimization theory was verified through multiple experiments, which improved the efficiency of mirror manufacturing to a greater extent, laying the theoretical foundation for subsequent work.

Additionally, we conducted a complete polishing experiment with the pre-polished mirror, and the final surface RMS reached $1/30\,\lambda$. The MRF equipment was used to complete the remaining finishing work. The final polished result is shown in the surface map in Fig. 15, which illustrates a good surface shape. Moreover, the introduction of pre-polishing shortens the polishing time of the MRF equipment, which improves the efficiency of complete polishing.

4.2.3 *Comparative experiment*

To verify the efficiency of our proposal further, we used identical K9 plane glass with a diameter of 140 mm to conduct comparative experiments. Specifically, we designed four experiments that used the classical method, uniform speed swing, uniform acceleration swing, and the uniform B-spline swing. The total polishing duration for each experiment was counted, and the results are presented in Fig. 16. The statistical results indicate that the total polishing duration of the pre-polishing group was 1.5 to 2.7 times shorter than that of the classical polishing group, which significantly reduced the calculation amount and complexity of deterministic polishing in the polishing stage. In addition, the duration of the experiment using the uniform B-spline as the velocity characteristic curve is significantly shorter than that of the experiment using the uniform acceleration swing, which further proves the efficiency of the proposed pre-polishing method.

The grating path was also used for tool mark comparison. To demonstrate the tool marks more intuitively, we culled and hid the unrelated part of the central area on the surface map, which does not affect the surface data or the result. A surface map of the grating path is shown in Fig. 17, which depicts that tool marks are more noticeable than that of the uniform B-spline

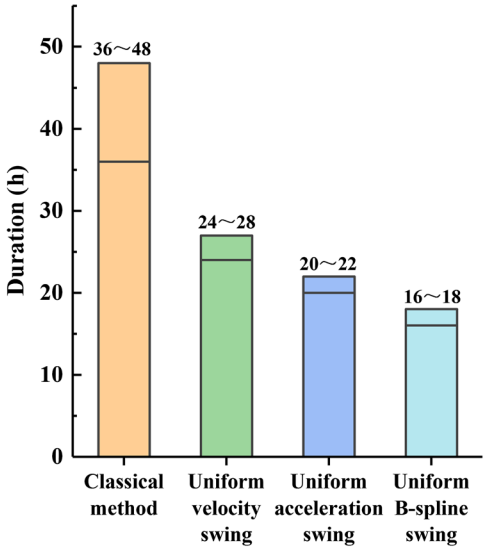

Fig. 16 Comparison of polishing duration.

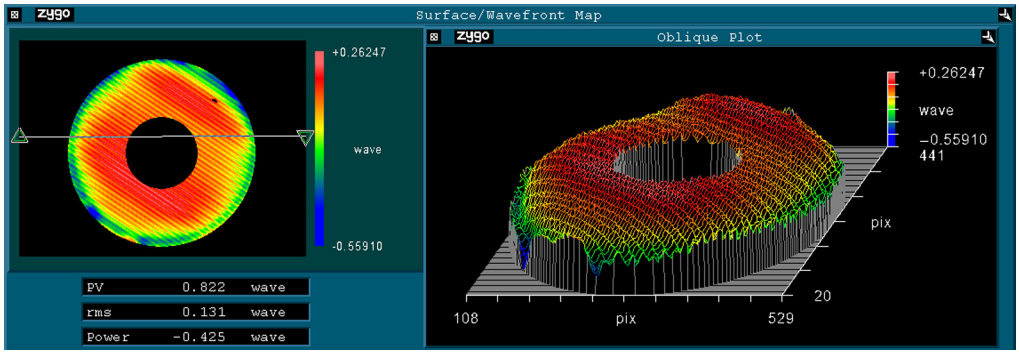

Fig. 17 Result of grating path polishing.

swing, causing a wider and deeper edge effect. The use of a conventional path also induces the early occurrence of mid-spatial frequency error, moving the processing wall forward. Excessive path points for polishing large-size mirrors cause many problems, such as errors and faults that occur in various types of control cabinets. In contrast, the simplified path point set of our proposed method enables a more stable operation of the robot, ensuring polishing accuracy.

5 Conclusions

In this study, we proposed a simple optical pre-polishing method; the parameters for several indicators were optimized to realize uniform removal, providing an excellent basic surface shape for the formal polishing stage. To achieve uniform removal, the pre-polishing optimization mainly focused on overlap rate, during which the actual characteristics and technical indicators of the polishing equipment were considered, particularly for the industrial robot. The optimization process realizes real-time verification of polishing results through simulation machining programming. The experimental results indicate that the variable-speed swing composite path can effectively reduce the complexity of pre-polishing and that the versatility of equipment in different process stages can be maximized. This path is also beneficial for subsequent polishing, by which the number of iterations can be reduced.

We conducted multiple experiments to verify the proposed and the theoretical optimization process. While realizing the $1/15\,\lambda$ RMS of the surface shape, our proposed method can maintain the basic surface shape of the milling stage and reduce the potential tool marks, benefiting

industrial robots used in optical batch manufacturing. Furthermore, the addition of pre-polishing can effectively shorten the polishing procedure and improve the efficiency of the entire process. In addition to industrial robots, other CNC equipment can also implement pre-polishing to increase the efficiency of large-diameter optical glass manufacturing, which is of great significance for batch manufacturing.

Despite the above research findings, certain problems concerning edge and center effects were not fully considered, which might pose a detrimental obstruction to the procedure. Therefore, our future research will focus on these problems, paving the way for future research and innovations in optical manufacturing.

Acknowledgments

We would like to thank Editage and ZillionZestEdit for English language editing. The research was funded by the West Light Foundation of the Chinese Academy of Sciences (XAB2016A10) and Key Research and Development Projects of Shaanxi Province, China (2018ZDXM-GY-105). The authors declare no conflicts of interest.

References

1. Z. B. Xia et al., "Advances in polishing of optical freeform surfaces: a review," *J. Mater. Process. Technol.* **286**, 116828 (2020).
2. A. Mohammad, J. Hong, and D. W. Wang, "Design of a force-controlled end-effector with low-inertia effect for robotic polishing using macro-mini robot approach," *Rob. Comput. Integr. Manuf.* **49**, 54–65 (2018).
3. A. Sidpara, "Magnetorheological finishing: a perfect solution to nanofinishing requirements," *Opt. Eng.* **53**(9), 092002 (2014).
4. T. Y. Wang et al., "Study on an effective one-dimensional ion-beam figuring method," *Opt. Express* **27**(11), 15368–15381 (2019).
5. C. Y. Shi et al., "Ultra-precision figuring using submerged jet polishing," *Chin. Opt. Lett.* **9**(9), 092201 (2011).
6. P. Dumas et al., "Complete sub-aperture pre-polishing & finishing solution to improve speed and determinism in asphere manufacture," *Proc. SPIE* **6671**, 667111 (2007).
7. S. R. Kiontke and R. Steinkopf, "Aspherical manufacturing in terms of accuracy, efficiency, and surface forms based on practical experiences," *Proc. SPIE* **7102**, 71020D (2008).
8. G. Zhong et al., "Influence of pre-polishing process on site flatness values of polished wafers," *Mater. Sci. Semicond. Process.* **68**, 15–20 (2017).
9. J. Chaves-Jacob, J. M. Linares, and J. M. Sprauel, "Control of the contact force in a pre-polishing operation of free-form surfaces realised with a 5-axis CNC machine," *CIRP Ann.-Manuf. Technol.* **64**(1), 309–312 (2015).
10. C. Wang et al., "Improved semirigid bonnet tool for high-efficiency polishing on large aspheric optics," *Int. J. Adv. Manuf. Technol.* **88**(5–8), 1607–1617 (2017).
11. X. L. Ke et al., "Tentative investigations on reducing the edge effects in pre-polishing the optics," *Appl. Sci.-Basel* **10**(15), 5286 (2020).
12. B. Zhong et al., "Evaluation and compensation of a kinematic error to enhance prepolishing accuracy for large aspheric surfaces by robotic bonnet technology," *Opt. Express* **28**(17), 25085–25100 (2020).
13. F. Prochaska et al., "Zeeko precession for free-form polishing," *Proc. SPIE* **10151**, 101510O (2016).
14. J. Liu et al., "Path planning and parameter optimization of uniform removal in active feed polishing," *Opt. Eng.* **54**(6), 065101 (2015).
15. Y. Feng et al., "Optimal strategy for fabrication of large aperture aspheric surfaces," *Appl. Opt.* **53**(1), 147–155 (2014).
16. K. Wu et al., "Dynamic performance of industrial robot with CNC controller," *Int. J. Adv. Manuf. Technol.* **90**(5–8), 2389–2395 (2017).

17. J. ZwierzchowskiIT/ASCR, "A device for automatic robot tool center point (TCP) calibration adjustment for the ABB industrial robots," in *23rd Int. Conf. Eng. Mech.*, p. 1138 (2017).
18. E. Fess et al., "Developments in precision optical grinding technology," *Proc. SPIE* **8884**, 88840L (2013).
19. C de Boor, "On calculating with B-splines," *J. Approx. Theory* **6**, 50–62 (1972).
20. M. G. Cox, "The numerical evaluation of B-splines," *J. Inst. Math. Appl.* **10**, 134–149 (1972).
21. H. X. Xu and Q. Q. Hu, "Approximating uniform rational B-spline curves by polynomial B-spline curves," *J. Comput. Appl. Math.* **244**, 10–18 (2013).
22. G. M. Bone and M. A. Elbestawi, "Active end effector control of a low precision robot in deburring," *Rob. Comput. Integr. Manuf.* **8**(2), 87–96 (1991).
23. D. W. Kim et al., "Parametric modeling of edge effects for polishing tool influence functions," *Opt. Express* **17**(7), 5656–5665 (2009).

Liangxiao Zhao is currently a PhD candidate at Xi'an Institute of Optics and Precision Mechanics of CAS and the University of Chinese Academy of Sciences. He received his BS degree in mechanical engineering from Taiyuan University of Technology in 2016. His research interests include robot-based optical grinding and polishing, as well as computer-controlled optical surfacing techniques. He is a student member of SPIE.

Jian Zhang is currently an associate research fellow at Xi'an Institute of Optics and Precision Mechanics of CAS. He received his MS degree from Xidian University in 2007. His research interests include robot application, advanced optical precision equipment design, and precision optical manufacturing.

Limin Gao is currently a research fellow at Xi'an Institute of Optics and Precision Mechanics of CAS. He received his BS degree from Zhejiang University in 1988, and his MS and PhD degrees in optical engineering from Xi'an Institute of Optics and Precision Mechanics of CAS in 1991 and 2004, respectively. His research interests include the design and application of optoelectronic measure equipment and high-power laser measurement and its application. He is a member of SPIE.